Self-assembly, antimicrobial activity, and membrane interactions of arginine-capped peptide bola-amphiphiles

ACS APPLIED BIO MATERIALS Cite This: ACS Appl. Bio Mater. XXXX, XXX, XXX−XXX

Article

www.acsabm.org

Self-Assembly, Antimicrobial Activity, and Membrane Interactions of Arginine-Capped Peptide Bola-Amphiphiles

Charlotte J. C. Edwards-Gayle,[†,⊥] Valeria Castelletto,[†] Ian W. Hamley,*[,†] Glyn Barrett,[‡] Francesca Greco,[†] Daniel Hermida-Merino,[§] Robert P. Rambo,[⊥] Jani Seitsonen,[¶] and Janne Ruokolainen[¶]

[†]School of Chemistry, Food Biosciences and Pharmacy, University of Reading, Whiteknights, Reading RG6 6AD, U.K.

[‡]School of Biological Sciences, University of Reading, Reading RG6 6UR, U.K.

[§]ESRF-The European Synchrotron, 38043 Grenoble Cedex 9 France

[⊥]Diamond Light Source, Harwell Science and Innovation Campus, Didcot, Oxfordshire OX11 0DE, U.K.

[¶]Department of Applied Physics, Aalto School of Science, P.O. Box 15100, FI-00076 Aalto, Finland

Supporting Information

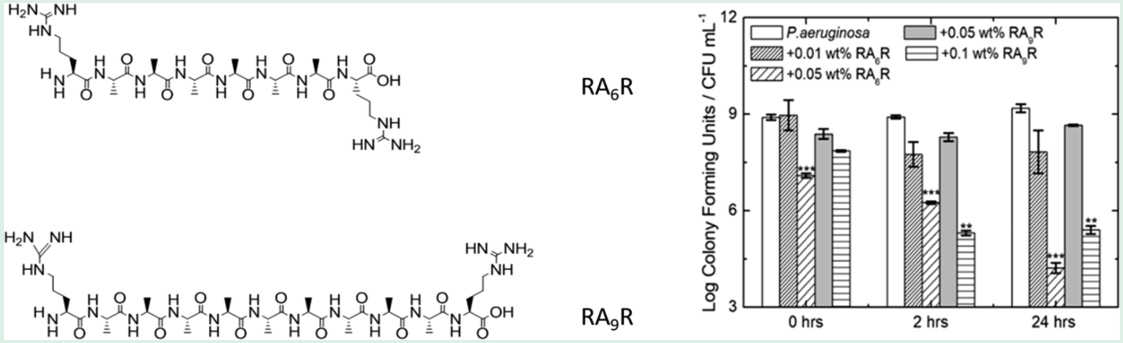

ABSTRACT: The self-assembly and antimicrobial activity of two novel arginine-capped bola-amphiphile peptides, namely RA_6R and RA_9R (R, arginine; A, alanine) are investigated. RA_6R does not self-assemble in water due to its high solubility, but RA_9R self-assembles above a critical aggregation concentration into ordered nanofibers due to the high hydrophobicity of the A_9block. The structure of the RA_9R nanofibers is studied by cryogenic transmission electron microscopy (cryo-TEM) and small-angle X-ray scattering (SAXS). Circular dichroism spectroscopy shows that both RA_6R and RA_9R adopt coil conformations in water at low concentration, but only RA_9R adopts a β-sheet conformation at high concentration. SAXS and differential scanning calorimetry are used to study RA_6R and RA_9R interactions with a mixed lipid membrane that models a bacterial cell wall, consisting of multilamellar 1,2-dipalmitoyl-*sn*-glycero-3-phosphoglycerol/1,2-dipalmitoyl-*sn*-glycero-3-phosphoethanolamine vesicles. Cytotoxicity studies show that RA_6R is more cytocompatible than RA_9R. RA_6R has enhanced activity against the Gram-negative pathogen *P. aeruginosa* at a concentration where viability of mammalian cells is retained. RA_9R has little antimicrobial activity, independently of concentration. Our results highlight the influence of the interplay between relative charge and hydrophobicity on the self-assembly, cytocompatibility, and bioactivity of peptide bola-amphiphiles.

KEYWORDS: *peptides, antimicrobial peptides, antibacterials, self-assembly, lipid membranes*

INTRODUCTION

The increasing occurrence of antibiotic resistant pathogens is leading to an urgent need to discover or design novel therapeutics to combat this issue. One important class of therapeutics is antimicrobial peptides. Antimicrobial peptides are attractive since many are expressed naturally, and this can be used as a basis for novel compounds and also due to their ease of biofunctionalization and biocompatibility.[1−3] Many organisms, for example, fungi, have naturally evolved host defense antimicrobial peptides, which can be used as actives themselves, or form the basis of designed synthetic materials. Antimicrobial peptides with the ability to self-assemble may be active without the need for carrier molecules.

A class of peptide with strong self-assembly properties are surfactant-like peptides (SLPs), initially developed by Zhang et al.[4−7] These peptides are short, consisting of a one or two charged residue headgroup, with a longer hydrophobic sequence as a tail group. Peptides with various cationic and anionic headgroups, and different hydrophobic amino acid tail

Received: March 4, 2019
Accepted: April 16, 2019
Published: April 16, 2019

Scheme 1. Structure of RA_6R, RA_9R, DPPG, and DPPE

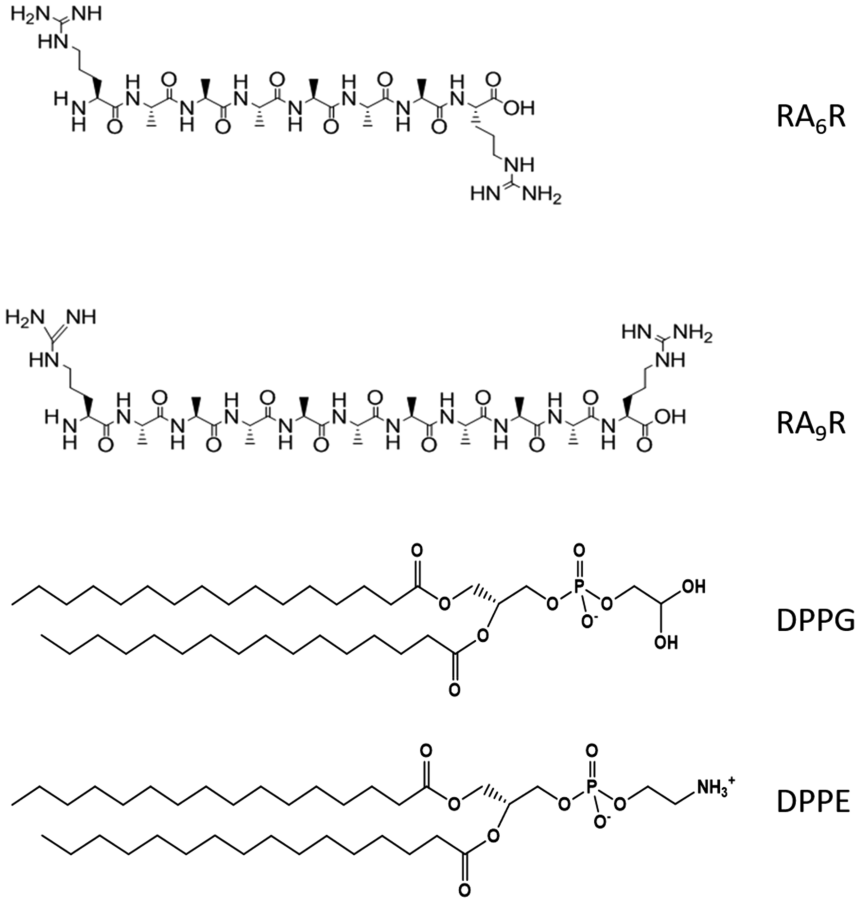

groups (including alanine, glycine and valine repeat units), have been studied. Previously our group has studied the conformation and nanostructure of SLPs including A_9R,[8] A_6H,[9] A_6K,[10] A_6R,[11] $capA_6R$,[12] A_6RGD,[13] and A_6D.[14] Self-assembly was observed for all of these peptides, above a critical aggregation concentration (*cac*), into a variety of structures including nanosheets, helical ribbons, fibrils, vesicles, nanotubes, and nanotapes, with a range of potential applications.

SLPs with cationic head groups have been shown to have antimicrobial activity.[15] A_6R was shown to have antimicrobial activity against *E. coli* and *S. aureus*, although interactions with zwitterionic mammalian lipid membrane model DPPC (1,2,dipalmitoyl-*sn*-glycero-3-phosphocholine) did not lead to breakup of these lipid vesicles.[16] Recently, the conformation, self-assembly, and interactions with lipid membranes were studied for $capA_6R$, which is capped at both termini (CONH-AAAAAAR-NH_2) to modulate electrostatic interactions. Interactions with zwitterionic membrane models (POPC/DOPC) [POPC: 2-oleoyl-1-palmitoyl-*sn*-glycero-3-phosphocholine, DOPC: 1,2-dioleoyl-*sn*-glycero-3-phosphocholine] and mixtures (POPG/POPE) [POPG: 2-oleoyl-1-palmitoyl-*sn*-glycero-3-phospho-rac-(1-glycerol) sodium salt, POPE: 2-oleoyl-1-palmitoyl-*sn*-glycero-3-phosphoethanolamine] containing the anionic POPG lipid were studied by SAXS and circular dichroism spectroscopy.[12] $CapA_6R$ was found to incorporate into the anionic membrane in a β-sheet conformation, in contrast to the uncapped peptide A_6R (NH_2-AAAAAAR−OH). $CapA_6R$ was found to have a strong selective antimicrobial activity against *Listeria monocytogenes*, compared to A_6R which shows nonselective activity. SLPs A_3K, A_6K, and A_9K were shown to assemble into increasingly ordered structures with increased length of the alanine hydrophobic motif.[15] Interestingly, the antimicrobial activity of these peptides also increased with the length of the hydrophobic motif, with A_3K showing no antimicrobial activity, and A_6K and A_9K showing activity against *E. coli* and *S.aureus*, which are Gram-negative and -positive, respectively.

Peptide bola-amphiphiles are a class of surfactant-like peptides. These peptides incorporate a charged residue at either end of the molecule. The self-assembly behavior of these SLPs has been investigated. The self-assembly of $I_2K_2I_2$ and KI_4K has been compared, and it was reported that the former does not aggregate whereas the latter aggregates into β-sheet nanotubes.[17,18] In another example, the self-assembly ability of arginine based bola-amphiphile RFL_4FR was investigated and it was found to form nanosheets through lateral association of the backbone and dried films were compatible with human corneal stromal fibroblast cells.[19] Recently our group studied the self-assembly, antimicrobial activity, and membrane interaction of a short bola-amphiphile consisting of arginine and alanine residues, RA_3R.[20] RA_3R was found to form a polyproline II (collagen-like) secondary structure, but it does not assemble in water probably due the solubility imparted by the R residues. RA_3R was found to induce strong correlation between anionic lipid bilayers through electrostatic interactions with POPG and demonstrates strong activity against the Gram-positive foodborne pathogen *L. monocytogenes*.

Here we investigate the self-assembly of the two peptide bola-amphiphiles RA_6R and RA_9R (shown in Scheme 1). This

DOI: 10.1021/acsabm.9b00172
ACS Appl. Bio Mater. XXXX, XXX, XXX−XXX

work follows on from the previous work on RA_3R and investigates the effect of longer hydrophobic alanine motifs on the self-assembling propensity, interactions with lipid membranes, biocompatibility, and antimicrobial activity. The self-assembly of RA_6R and RA_9R is studied in aqueous solution, and interactions with lipid vesicles DPPG and DPPG/DPPE at different ratios are investigated. In water, DPPG (1,2-dipalmitoyl-*sn*-glycero-3-phosphoglycerol) is anionic and DPPE (1,2-dipalmitoyl-*sn*-glycero-3-phosphoethanolamine) is zwitterionic (Scheme 1). Phosphoglycerol (PG) and phosphoethanolamine (PE) lipids are commonly found in bacterial cell walls, in contrast to mammalian cell membranes, which contain a substantial component of phosphocholine (PC) and PE lipids, but not anionic PG lipids.[21−25] Different bacteria species have distinct compositions of PG and PE lipids in their membranes,[26,27] and there are also significant membrane architecture differences between Gram-positive and Gram-negative bacteria.[28,29] We have selected DPPG/DPPE lipid mixtures for the present study because both lipids have accessible melting temperatures (in contrast to POPG used in our previous studies which has $T_m = -2$ °C). This lipid system has been utilized in previous studies on antimicrobial peptide−membrane interactions.[23,30] Finally, we examine the cytocompatibility and antimicrobial activity of RA_6R and RA_9R. In contrast with the previous study on RA_3R,[20] we include an examination of antibacterial activity against *Pseudomonas* species, an important class of animal and plant pathogen.

METHODS

Materials. Peptides RA_6R and RA_9R were supplied by Biomatik (Cambridge, Ontario, Canada). RA_6R purity was 98.86% by HPLC using an Inertsil ODS-SP column with acetonitrile/water (0.1% TFA) gradient. RA_6R molar mass by ESI-MS was 757.45 g mol^{-1} ($M+H^+$, 756.87 g mol^{-1} expected). RA_9R purity was 96.56% by HPLC using an Inertsil ODS-SP column with acetonitrile/water (0.1% TFA) gradient. RA_9R molar mass by ESI-MS was 970.65 g mol^{-1} ($M+H^+$, 970.11 g mol^{-1} expected). Solutions containing pure peptide in water were made by dissolving weighed amounts of peptide in water, which were left to equilibrate for 3 h. The pH was measured as a function of peptide concentration, and the data are shown in Figure S1. Lipids DPPG and DPPE were obtained from Sigma-Aldrich. Details of multilamellar lipid vesicle preparation are given below.

Fluorescence Assays. The presence of any critical aggregation concentration (*cac*) was assayed using fluorescence probes, measuring spectra for a series of peptide concentrations. Fluorescence spectra were recorded with a Varian Cary Eclipse fluorescence spectrometer with samples in 4 mm inner width quartz cuvettes. ThT was used to determine the *cac* of RA_9R, as it is sensitive to the formation of amyloid fibrils at the *cac*.[31−35] ThT assays were performed using 5.0×10^{-3} wt % solution to solubilize the peptide. Spectra were recorded between 460 and 600 (λ_{ex} = 440 nm). ANS (8-anilinonaphthalene-1-sulfonic acid) was further used to examine whether there is a *cac* for RA_6R. ANS is a fluorescent probe used to determine the formation of molecular hydrophobic environments in solution and can be used to determine the *cac* independent from self-assembly into amyloid fibers.

Circular Dichroism (CD) Spectroscopy. CD spectra were recorded as described previously.[8] Samples containing 1 wt % RA_6R or RA_9R in pure H_2O were pipetted into 0.01 mm path length quartz plaque cells or 0.1 mm quartz cuvettes.

Fourier Transform Infrared (FTIR) Spectroscopy. Spectra were recorded as described previously.[8] Aliquots containing 80 μL of (1−5) wt % RA_6R or RA_9R in D_2O were prepared and added to a PEARL liquid cell.

Cryogenic Transmission Electron Microscopy (Cryo-TEM). Samples were imaged as described previously.[8]

Rheology. Measurements were carried out as described previously.[8]

Liposome Preparation. Liposome vesicles were prepared using the thin-layer hydration method. Weighed quantities of DPPG and DPPE were dissolved in chloroform, and thin lipid films were prepared as described previously.[8] After this, lipids were resuspended in water at 0.5 wt % lipid, heated at 65 °C, above their lipid melting temperature, T_m, and vortexed for 5 min. Liposome mixtures were then left to equilibrate for 3 h before experiments. DPPG/DPPE vesicles were prepared using this method at different molar ratios of 1:3, 1:1, 3:1, and 1:0 DPPG:DPPE. Peptide/lipid mixtures were made by adding enough peptide powder to resuspended lipids to obtain a final concentration of either 0.08 or 0.25 wt % peptide. Peptide/lipid samples were then heated above the T_m and vortexed for 5 min and finally left to equilibrate for 3 h before experiments.

Nano Differential Scanning Calorimetry (Nano-DSC). Differential scanning calorimetry measurements were carried out using a nanoDSC, DSC TA-Q200 instrument. Aliquits of 600 μL of lipid mixtures at 0.5 wt % with and without 0.08 wt % peptide were degassed for 10 min before being pipetted into the DSC sample cell. An amount 600 μL of water was pipetted into the reference cell. The temperature range measured was 20 to 80 °C for DPPG/DPPE mixtures and 20 to 60 °C for DPPG alone. The scan rate was 1 °C per minute at pressure of 3 bar. Background subtraction, main phase transition temperature, and the transition enthalpy, ΔH, were calculated using nanoanalyse software.

Small-Angle X-ray Scattering (SAXS). Data from solutions were collected on the bioSAXS beamlines B21 (Diamond Light Source, UK) and ID02 (ESRF, Grenoble). At the former, liposome and peptide samples were loaded into PCR tubes in an automated sample changer, and measurements were performed as described previously.[8] Data were processed using ScÅtter[36] and are presented as a function of $q = 4\pi \sin \theta/\lambda$. At the ESRF (ID02), 200 μL of sample was manually loaded into a glass capillary with a 2 mm internal radius. The beamline operated with λ = 1 Å and a sample−detector distance 1.47 m. The SAXS data from B21 and ID02 were fitted using model form factors using the software SASfit.[37] SAXS from hydrogels was collected on beamline BM26B (DUBBLE) at the ESRF. On BM26B, measurements on gels were performed as described previously.[8]

Cell Viability Assays. In vitro cell culture was conducted using 161Br (European Collection of Authenticated Cell Cultures, ECACC) cells, a human skin fibroblast cell line. Cells were maintained in a humidified atmosphere at 37 °C, 5% CO_2, and cultured in EMEM (Eagle's minimum essential medium), with 2 mM glutamine, enriched with 15% fetal bovine serum (FBS) and 1% nonessential amino acids (NEAA).

Potential cytotoxicity effects of RA_6R and RA_9R were examined using an MTT (3-(4,5-dimethylthiazol-2-yl)-2,5-diphenyltetrazolium bromide) assay. Cells were seeded into a 96-well plate at 4×10^4 cells/mL and allowed to adhere for 24 h in 100 μL of complete medium. After this, peptides were dissolved in complete medium, and 100 μL of either complete medium or peptide solution was added to give either control solution (complete medium only) or peptide solutions with concentrations in the range 0.05−5 mg/mL.

Cells were incubated for 67 h. Following this, 20 μL of MTT (5 mg/mL, in PBS) was pipetted into each well plate and allowed to incubate for 5 h. After a further 5 h (corresponding to a total of 72 h treatment), the solution was removed from the wells and replaced with 100 μL of DMSO per well to dissolve the formazan crystals. Absorbance was measured as described previously.[8]

Antimicrobial Assays. The antimicrobial assays were performed with three types of bacteria, *Escherichia coli*,[38] *Staphylococcus aureus*,[39] and *Pseudomonas aeruginosa*.[40] Culture methods are as described previously.[8]

RESULTS AND DISCUSSION

We first characterize the self-assembly of RA_6R and RA_9R in water using CD, FTIR, XRD, SAXS, and cryo-TEM. We then study the interaction of RA_6R and RA_9R with model bacterial

DOI: 10.1021/acsabm.9b00172
ACS Appl. Bio Mater. XXXX, XXX, XXX−XXX

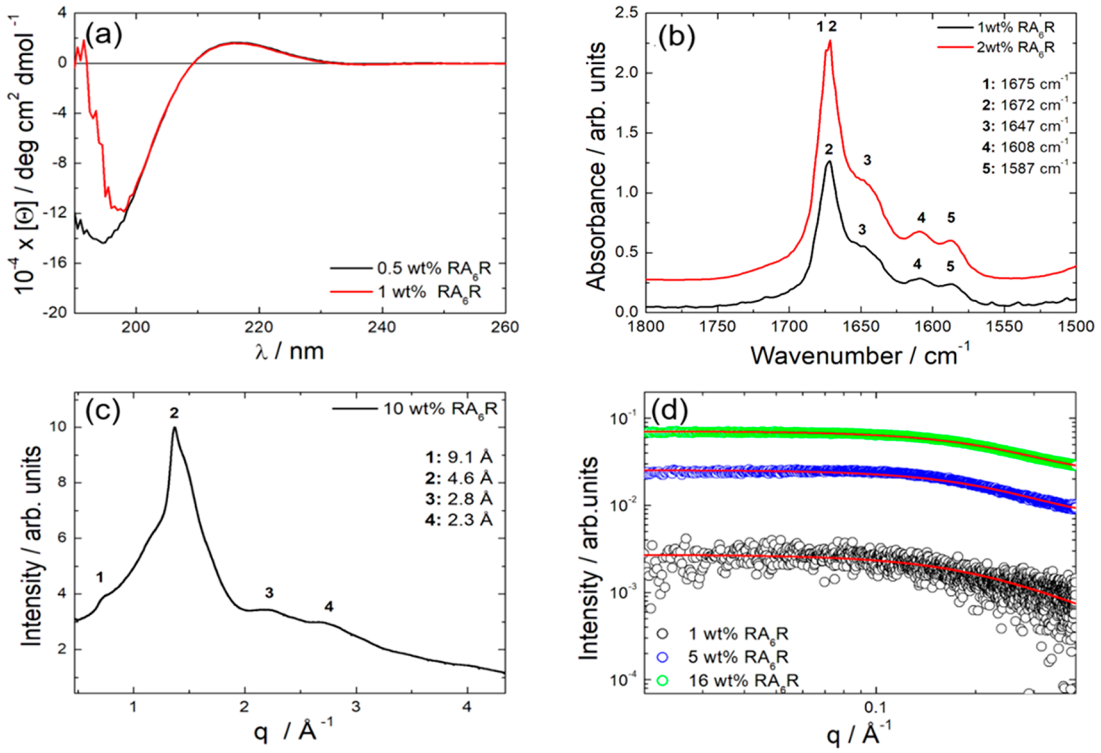

Figure 1. Conformational and structural characterization of RA_6R in solution (a) CD and (b) FTIR spectra; (c) XRD profile; and (d) SAXS profiles. The concentration of the solutions is indicated in the graphs, the full lines in panel d correspond to the fitting of the SAXS data as described in the text.

membrane walls represented by DPPG/DPPE multilamellar vesicles. Finally, we study the cytotoxicity and antimicrobial activity of RA_6R and RA_9R. We discuss our results in terms of the interplay between molecular structure, peptide self-assembly and biological activity.

Peptide Self-Assembly. ANS and ThT fluorescence assays were performed to determine the *cac* for RA_6R in water (Figure S2), as they probe hydrophobic collapse (ANS) or amyloid fibril formation (ThT).[32,41] ANS and ThT assays provided no evidence of peptide aggregation up to 1 wt % RA_6R since there were no discontinuities in the fluorescence spectra for either fluorescence probe (Figure S2). In fact, CD, FTIR, XRD, and SAXS experiments, performed to study the secondary structure of RA_6R in water, indicate that this peptide does not form defined aggregates.

The CD spectra for (0.5−1) wt % RA_6R are characterized by a broad positive maximum at ∼220 nm and a deep negative band around 190 nm (Figure 1a) and can be assigned to a polyproline II (PPII) conformation.[20,42−46] The FTIR spectrum for a 1 wt % sample (Figure 1b) shows bands at 1672 cm^{-1}, 1647 cm^{-1}, 1608 cm^{-1}, and 1587 cm^{-1}, the first of which can be assigned to TFA counterions in solution,[47,48] the 1647 cm^{-1} peak is due to disordered structure, and the latter two peaks can be assigned to arginine side chain vibrations.[49,50] A shoulder peak at 1675 cm^{-1} is observed for 2 wt % RA_6R, which is characteristic of short peptides with a PPII structure, in agreement with the CD spectra (Figure 1a).[51,52] The XRD profile (Figure 1c) shows a peak at 4.6 Å corresponding to a disordered side-to-side packing of the RA_6R molecules.[11]

SAXS data for RA_6R (Figure 1d) show the features of peptide monomers. The SAXS curves were fitted to a generalized Gaussian coil model, corresponding to coil-like molecules in solution with different degrees of solvation. The parameters fitted using the generalized Gaussian model were the radius of gyration of the peptide R_g and the Flory exponent ν. Fittings in Figure 1d provided R_g = 7.0 Å, 7.16 Å, 6.94 Å and ν = 0.64, 0.24, 0.20 for 1, 5, and 15 wt % RA_6R, respectively. This set of parameters implies that RA_6R is in a swollen conformation at 1 wt % and a relatively folded conformation at 5 and 16 wt %. Cryo-TEM images of RA_6R solutions show the formation of occasional clusters of monomers (results not shown).

The self-assembly of RA_9R in water was studied following the same procedure used for RA_6R. Results from the ThT assay (Figure 2a) shows that RA_9R aggregates into amyloid fibers[32] above a *cac* = (0.18 ± 0.03) wt %. CD shows that the peptide adopts a predominantly PPII like conformation up to 1 wt % but at higher concentration forms β-sheet structures (Figure 2b). The PPII structure clearly persists at concentrations above the *cac* from the ThT assay. The secondary structure at 1 wt % remains predominantly PPII like upon heating (Figure S3a), but changes into a β-sheet conformation, characterized by the minimum near 216 nm, upon drying the sample (Figure S3b). The FTIR spectrum for 1 wt % RA_9R (Figure 2c) shows peaks at 1672 cm^{-1}, 1647 cm^{-1}, 1608 cm^{-1}, and 1587 cm^{-1}, which are respectively assigned to modes associated with TFA counterions,[47,48] disordered structure, and arginine vibrational modes,[49,50] as stated earlier. Upon increasing concentration to 5 wt %, a strong peak develops at 1622 cm^{-1}, which is due to β-sheet structure.[50,53]

The XRD profile of RA_9R (Figure 2d) shows a 5.32 Å reflection, which can be assigned to the packing of polyalanine β-sheets,[12] with interstrand and intrastrand spacings of 4.32 Å, 3.72 Å, 2.83 Å, 2.39 Å, and 2.26 Å. Interestingly, we observed that RA_9R has the ability to form a weak gel at a concentration of 5 wt %, which is likely to result from the change in

DOI: 10.1021/acsabm.9b00172
ACS Appl. Bio Mater. XXXX, XXX, XXX−XXX

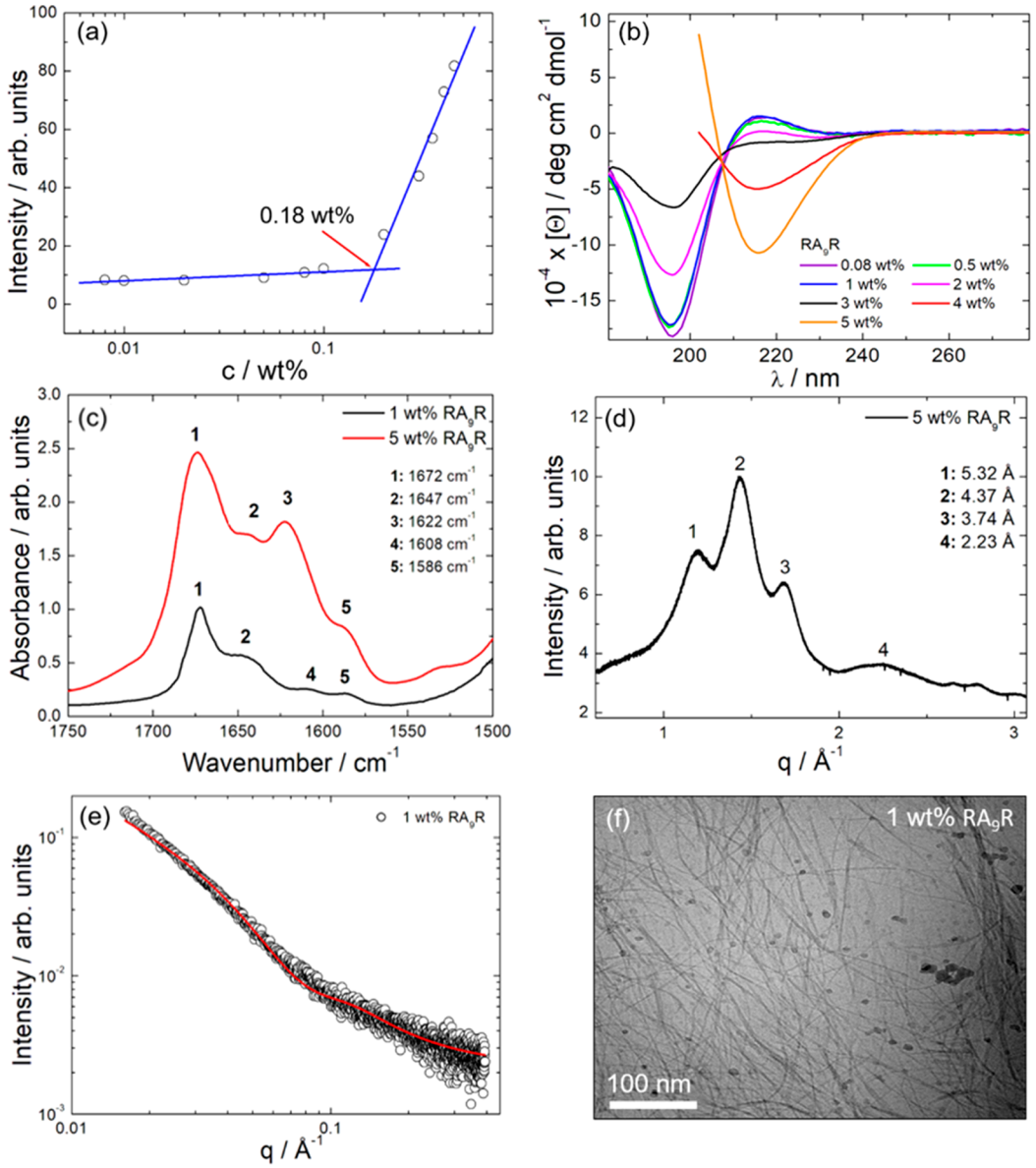

Figure 2. RA_9R self-assembly in water: (a) concentration dependence of ThT fluorescence intensity at λ_{em} = 520 nm. (b) CD spectra, (c) FTIR spectra, (d) XRD data, (e) SAXS profiles, and (f) cryo-TEM image for a 1 wt % sample above the *cac*. The concentration of the solutions is indicated in the graphs. The red line in panel e corresponds to the fitting of the SAXS data as described in the text.

secondary structure from PPII to β-sheet shown by CD. The properties of the gel will be discussed shortly.

SAXS data measured for 1 wt % RA_9R, were modeled using the form factor of a long cylindrical shell (Figure 2e; fitting parameters listed in Table S1). The fitted parameters are the core radius R (with polydispersity ΔR), the shell thickness D_r, and the scattering length density of the core, shell, and solvent η_{core}, η_{shell}, and η_{solv}. The extracted parameters, $R \pm \Delta R$ = (15 ± 10) Å and D_r = 3 Å, indicate that the cylinder core radius is less than the length of the oligoalanine A_9 sequence = 28.8 Å (spacing per residue in a parallel β-sheet is 3.2 Å), while the external shell has a dimension similar to one arginine unit. This result shows that there is an overlap of the alanine chains within the core of the fibers, with the arginine residue exposed at the surface of the fibers. Cryo-TEM confirms the presence of fibers with an average diameter of 7.6 nm (Figure 2f).

RA_9R forms a self-standing gel at 10 and 15 wt %. Figure S4a shows the SAXS data measured for 15 wt % RA_9R along with the rheological data including the hydrogel linear regime (Figure S4b) and frequency dependence of the storage (G') and loss (G'') moduli within the linear regime (oscillatory stress 100 Pa, Figure S4c). The fitting of the SAXS data in Figure S4a using the same form factor used in Figure 2e (parameters listed in Table S1) shows that the RA_9R hydrogel comprises a network of fibers similar to those found in solution.

Overall, our results indicate that, similarly to previously studied peptide RA_3R,[20] RA_6R does not self-assemble in water. It is likely that the flexibility of the PPII helical structure together with the solubility of the arginine residues does not favor RA_6R self-assembly. Increasing the length of the hydrophobic central block decreases the solubility of the molecule and allows for the self-assembly of RA_9R into β-sheet fibrils at sufficiently high concentration.

Interactions with Liposomes. Next, we examined the interactions of RA_6R and RA_9R with a model bacterial mixed

DOI: 10.1021/acsabm.9b00172
ACS Appl. Bio Mater. XXXX, XXX, XXX−XXX

lipid membrane, represented by DPPG/DPPE vesicles. DPPG is an anionic lipid, whereas DPPE is zwitterionic and both are commonly found in bacterial membranes.[15,23] We selected DPPG and DPPE because their melting temperatures (T_m) 41 °C (DPPG) and 63 °C (DPPE) are well apart and can be accessed with conventional instruments.[23] We examined 0.5 wt % DPPG/DPPE vesicles with ratios 3:1, 1:1, or 1:3, with 0.08 wt % peptide. While 0.08 wt % peptide is in the range of concentrations used for the antimicrobial assays discussed below, higher concentrations of peptide led to DPPG/DPPE/peptide sample precipitation and therefore were excluded from this study. DSC has been previously used to investigate lipid demixing in binary lipid membranes, driven by the membrane interaction with charged peptides.[15,23]

DSC thermograms for the lipids alone (Figure 3) present well-defined peaks in the second heating ramps shown (with

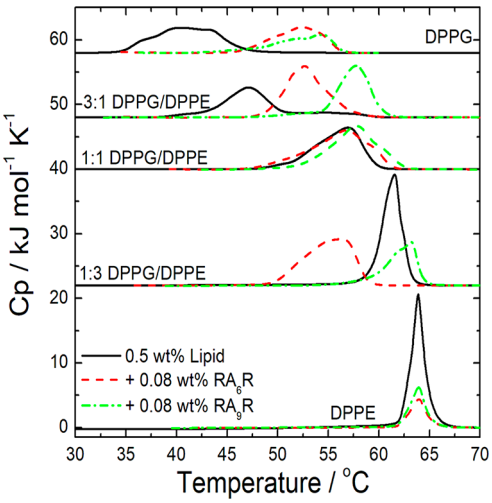

Figure 3. DSC scans showing second heating of DPPG/DPPE lipid mixtures with or without peptide. Scans for peptides mixed with lipids are plotted as dashed lines, and data for the lipid mixtures (without peptide) by the solid lines. The corresponding sample compositions are indicated in the plots.

the exception of the data for DPPG, which shows a broad transition for reasons discussed below), as observed previously.[23,54] To compare the influence of RA_6R and RA_9R on the thermotropic phase behavior of the DPPG/DPPE mixtures, the thermodynamic parameters, namely the main transition temperature (T_m) and the transition enthalpy ΔH, were calculated as an indication of the transition cooperativity. These parameters are listed in Table 1. For DPPE, the T_m stays within 0.1 °C of the lipid T_m, indicating little peptide binding, however there is a decrease in ΔH by 23.24 kJ mol^{-1} and 27.79 kJ mol^{-1} upon addition of RA_6R and RA_9R, respectively. This indicates that there is some interaction between the peptides and DPPE, which promotes a lowering of the energy needed for DPPE to undergo the phase transition to the liquid phase.

DPPG alone shows a pretransition to the P_β ripple phase at about 35 °C and a main chain melting temperature (to the fluid state, L_α phase) of 40.5 °C in good agreement with previous measurements for DPPG.[24,55] In the presence of RA_6R, there is a shift in the melting temperature T_m to 52.4 °C, as expected from peptide binding to anionic lipid.[24] RA_9R also causes an increase in the main T_m. A lowering of phase transition enthalpy is observed for DPPG mixed wityh peptide, where ΔH is reduced by 8.9 kJ mol^{-1} and 14.93 kJ

Table 1. Maximum Transition Temperature, T_m, and Enthalpy, ΔH, of Phase Changes Determined from Data Plotted in Figure 3

mixture	T_m (°C)	ΔH (kJ mol^{-1})
DPPE	63.86	37.11
DPPE + RA_6R	63.93	13.87
DPPE + RA_9R	63.97	9.32
0.5 wt % DPPG/DPPE 3:1	47.13	29.36
0.5 wt % DPPG/DPPE 3:1 + 0.08 RA_6R	53.64	38.63
0.5 wt % DPPG/DPPE 3:1 + 0.08 RA_9R	57.73	32.24
0.5 wt % DPPG/DPPE 1:1	56.90	30.84
0.5 wt % DPPG/DPPE 1:1 + 0.08 RA_6R	56.78	34.61
0.5 wt % DPPG/DPPE 1:1 + 0.08 RA_9R	57.80	36.92
0.5 wt % DPPG/DPPE 1:3	60.77	37.52
0.5 wt % DPPG/DPPE 1:3 + 0.08 RA_6R	56.19	43.00
0.5 wt % DPPG/DPPE 1:3 + 0.08 RA_9R	61.54	37.49
DPPG	40.52	32.43
DPPG + RA_6R	52.42	23.53
DPPG + RA_9R	54.54	17.50

mol^{-1} for RA_6R and RA_9R, respectively. The increase in main transition temperature of 11.9 °C for RA_6R and 14.0 °C for RA_9R is likely caused by the charged arginine residues strongly binding to the anionic DPPG group, causing an increase in the main transition temperature. Moreover, the peaks for DPPG with added peptide are asymmetric in shape, with RA_9R showing a small second peak at 50.1 °C, which could be due to DPPG transitioning in steps into the L_β phase based on how much peptide is bound.

For the DPPG/DPPE 3:1 mixtures, there are increases in main chain transition temperature of 5.5 and 10.6 °C, respectively, for RA_6R and RA_9R, which places T_m for RA_6R at a similar value to that observed in the mixture with DPPG alone, suggesting some demixing could be occurring. The mixture with RA_9R has a higher main transition temperature than that of DPPG alone. There is an increase in ΔH for both peptides, indicating that the peptide is stabilizing the P_β phase. At a ratio of 1:1 DPPG/DPPE, there are no large changes in main transition temperature (~1 °C); however, RA_6R shows a small secondary peak at 60 °C showing evidence of DPPE-rich regions, which shows demixing may be occurring. Finally, in the mixtures with 1:3 ratio of DPPG/DPPE, RA_9R has an asymmetric peak with a T_m of 61.5 °C, which is comparable to that when only DPPE is present, suggesting demixing. RA_6R causes a decrease in transition temperature by 4.6 °C, suggesting formation of DPPE-depleted domains compared to the control lipid mixture.

CD was used to examine whether interactions of the peptides with DPPG/DPPE membranes influenced their secondary structure. These measurements were performed at room temperature, where the lipids are below T_m, that is, in the gel phase. This is relevant to studying antimicrobial peptide activity, as highlighted for example by Pimthon et al.[30] Figure 4 shows the CD spectra of the RA_6R and RA_9R (0.08 wt % peptide), compared to those in the presence of DPPG/DPPE lipid mixtures. RA_6R appears to retain a PPII coil conformation in the presence of lipids. The decreased molar ellipticity implies slight loss of structure. The molar ellipticity decreases with higher ratios of DPPG, and a disordered structure is observed for the solution of RA_6R with only DPPG, which is characterized by a 190 nm minimum and the loss of the 220 nm broad peak. This is perhaps due to the strong binding

DOI: 10.1021/acsabm.9b00172
ACS Appl. Bio Mater. XXXX, XXX, XXX−XXX

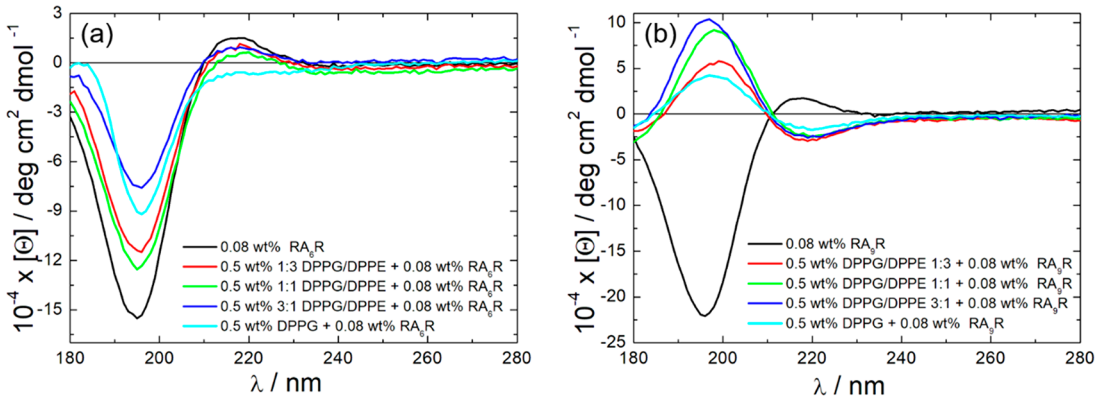

Figure 4. CD spectra for (a) RA_6R and (b) RA_9R peptides on their own or mixed with lipids, at the concentrations indicated.

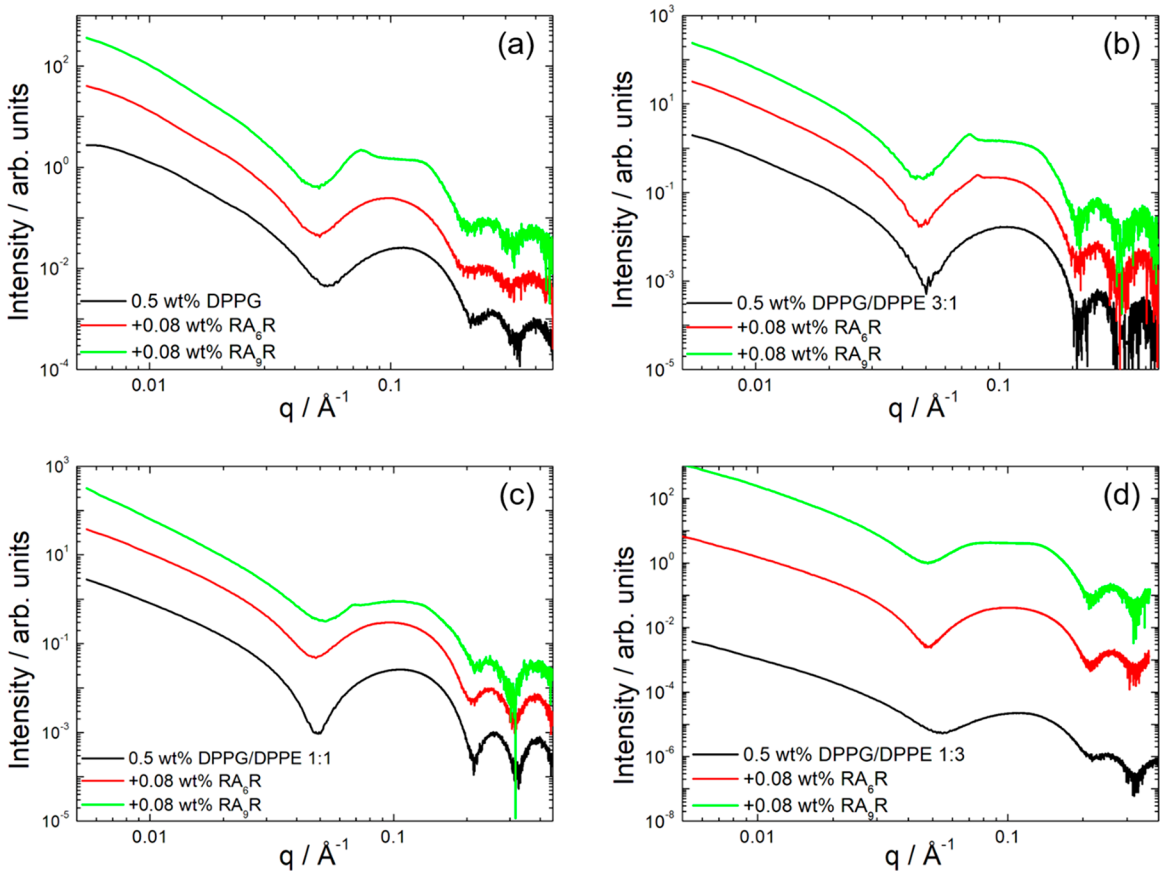

Figure 5. SAXS profiles for mixtures of lipids (total 0.5 wt %) and 0.08 wt % peptide. (a) DPPG:DPPE 1:0, (b) DPPG:DPPE 3:1, (c) DPPG:DPPE 1:1, (d) DPPG:DPPE 1:3.

between the ionic headgroup of the DPPG and the peptide inhibiting secondary structure formation.

Remarkably, the PPII secondary structure measured for pure RA_9R in solution changes into a β-sheet structure in the presence of lipid (Figure 4b). This shows that the DPPG/DPPE lipid membrane orders the peptide into a β-sheet secondary structure at a concentration of RA_9R below its *cac* (Figure 2a). A similar effect has previously been reported by us for $capA_6R$.[12] The population of RA_9R induced β-sheets increases as the DPPG content increases (Figure 4b), indicating that RA_9R binds more strongly to DPPG than to DPPE. One possible explanation for the transition to β-sheets in the presence of the lipid membranes is a local concentration enhancement of the peptide at the membrane interface since RA_9R does form β-sheet structure, but in bulk only at concentrations higher than the *cac* (Figure 2b).

SAXS was also used to examine the interactions of lipids with the peptides. SAXS data for lipids and peptides shown in Figure 5 were collected at 20 °C, which is in the gel L_β phase for all lipid mixtures. For the pure lipids, a broad peak positioned at approximately q = 1.5 nm^{-1} corresponds to unilamellar vesicles. SAXS data from temperature ramps in the range 20−50 °C for the peptides mixed with DPPG at two concentrations are shown in Figure S5, these data show particularly enhanced lipid bilayer correlations on heating at the higher peptide concentration studied (0.25 wt %).

DOI: 10.1021/acsabm.9b00172
ACS Appl. Bio Mater. XXXX, XXX, XXX−XXX

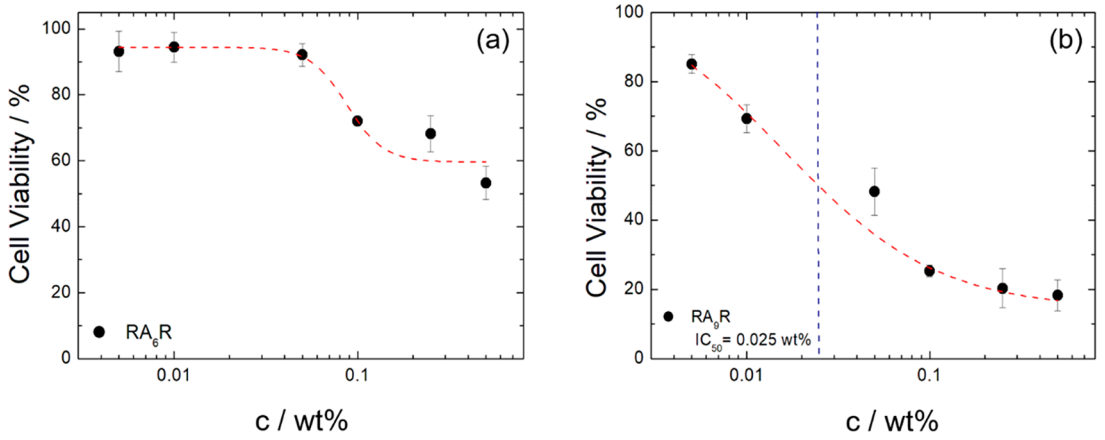

Figure 6. MTT assay showing the cytocompatibility of (a) RA_6R and (b) RA_9R with human skin fibroblasts.

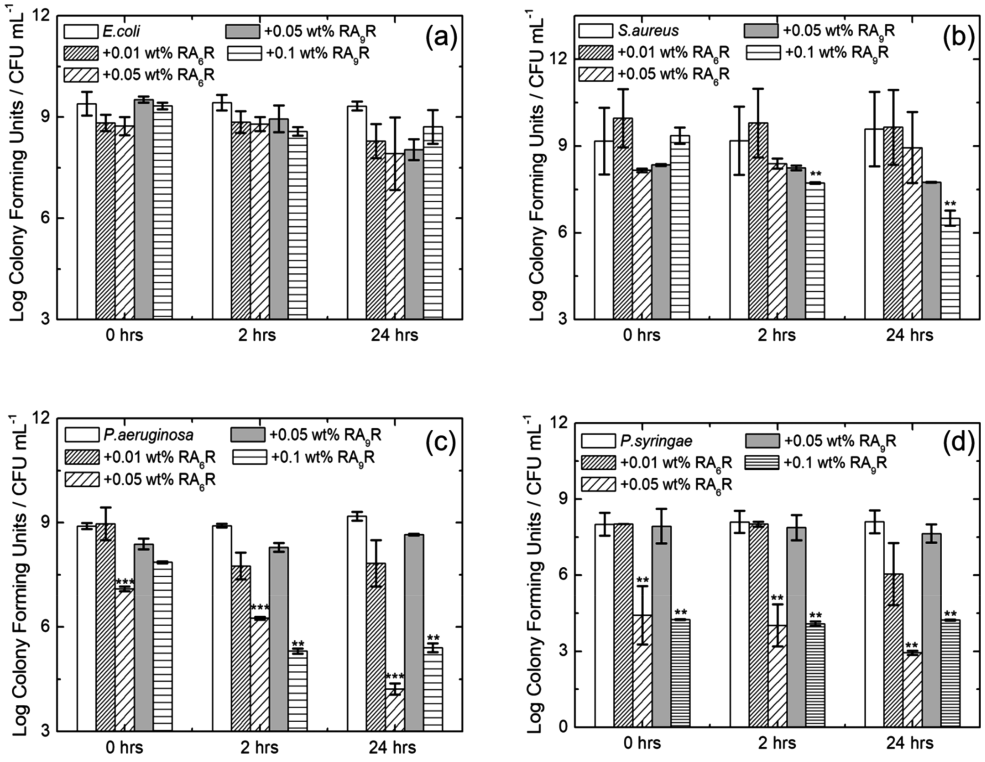

Figure 7. Antimicrobial activity against different bacteria, where time 0 is ~5 min from when the peptide is added to the solution. Peptide concentrations and bacteria types are indicated in the figure captions. (a) *E. coli*, (b) *S. aureus*, (c) *P. aeruginosa*, (d) *P. syringae*.

Upon addition of RA_9R, the SAXS data in Figure 5 show that some correlation between bilayers is induced, as indicated by the presence of small Bragg peaks. In contrast, RA_6R only causes a shift to lower q of the form factor minimum, that is, there is a slight increase in the bilayer spacing of the unilamellar vesicles. This implies that RA_9R causes membrane correlations due to the formation of β-sheet structure as concluded from CD results earlier. However, RA_6R does not change membrane correlations, but it does restructure the membranes, possibly due to interaction between the arginine residues and the charged DPPG head groups. In the DPPG/RA_9R mixture, the peptide induces two Bragg peaks with d-spacing values of 83.1 and 44.8 Å ($d = 2\pi/q_0$; q_0, coordinate for the peak maxima), consistent with a multilamellar structure. Cryo-TEM images of peptides in the presence of the lipid mixtures are shown in Figure S6. These images show the presence of some fibrils of RA_9R coexisting with vesicles; however, the SAXS signal is dominated by the contribution from the vesicles, as shown by the data in Figure 5.

Cytocompatibility and Antibacterial Activity. The results obtained with model DPPG/DPPE membranes suggest that RA_6R has little restructuring effect and may simply be adsorbed onto the lipid membranes, especially DPPG-rich ones. On the other hand, RA_9R undergoes a conformational switch in the presence of the gel phase of any of the DPPG/DPPE composition membranes investigated. These findings should be considered in any analysis of the interactions of the peptides with mammalian and bacterial cells, which have distinct lipid compositions (bacterial membranes have higher PE lipid contents).

To assess the cytocompatibility of the peptides, an MTT assay using human skin fibroblast cells was performed. Cell

DOI: 10.1021/acsabm.9b00172
ACS Appl. Bio Mater. XXXX, XXX, XXX−XXX

viability assays (Figure 6) show that RA_6R and RA_9R were tolerated by the cells up to 0.1 and 0.01 wt %, respectively (above 70% viability). The IC_{50} concentration was found to be 0.025 wt % for RA_9R, while for RA_6R, the IC50 was not observed in the concentration range studied. Since it has been established that RA_6R does not self-assemble, the increase in cytotoxicity with increasing peptide concentration could be associated with interactions of the peptide monomer with the lipid membrane. A similar peptide RA_3R also interacts with lipid membranes in the form of unassociated molecules due to interactions between the arginine residues and anionic or lipid head groups.[20] The cytotoxicity of RA_9R is higher than that of RA_6R at a given concentration, likely in some part due to the self-assembly of the fibrils, in which the arginine motif is presented at high density on the fibril surface. A further factor may be the increased hydrophobicity of RA_9R due to the increase in alanine sequence length.

To investigate the potential antimicrobial activity of these peptides, a range of common Gram-negative and Gram-positive bacteria were selected for initial screens using straightforward bacterial kill assays (counts of colony-forming units, CFUs). The Gram-positive microbe we selected was *S. aureus*, which is commonly found as part of the human microbiota and is an opportunist pathogen that can cause a range of infections including food poisoning, skin infections, and respiratory tract infections. The Gram-negative bacteria we selected included *E. coli*, which is a widely studied bacterium that often causes food-borne infection, and *P. aeruginosa*, which is an opportunist pathogen causing serious infections in cystic fibrosis patients, as well as having advanced multidrug resistant mechanisms and ability to cause hospital acquired infections through the formation of biofilms. We also examined *P. syringae*, a Gram-negative plant pathogen.

Antimicrobial assays were conducted against these three strains to assess the survival of *E. coli*, *S. aureus*, and *P. aeruginosa* in the presence of either control (water), RA_6R, or RA_9R. For RA_6R, we selected 0.05 and 0.1 wt % as peptide concentrations because at these concentrations the human cell viability is 92.5% (±3.4%) and 72.0% (±1.8%), respectively. For RA_9R, we were interested in how the peptide at a concentration below or above the IC_{50} concentration affected antimicrobial activity therefore the concentrations 0.01, 0.05, and 0.1 wt % were selected. The concentration 0.01 wt % is much lower than the *cac*, whereas 0.05 wt % is close to the concentration at which (according to CD spectra in Figure 4) the peptide forms a β-sheet structure in the presence of lipid membranes. The results from the antimicrobial assays are shown in Figure 7 and Figure S7.

There was no reduction in the bacterial colony count of *P. aeruginosa*, *E. coli*, or *S. aureus* at an RA_9R concentration of 0.01 wt % (Figure S6), showing that there is no antimicrobial activity under these conditions. When increasing the concentration to 0.05 wt %, there was a 0.5 log CFU reduction for *E. coli* after 24 h (Figure 7a). For *S. aureus*, there was a greater reduction of 1 log CFU after 2 h and 1.3 log CFU after 24 h (Figure 7b). For *P. aeruginosa* and *P. syringae*, there is no effect (Figure 7c,d). When increasing the concentration to 0.1 wt % peptide, there is a small, statistically insignificant reduction of 0.7 log of *E. coli* numbers when exposed to RA_9R. Interestingly, the reduction in colony forming units (CFU) after 24 h are 2.6, 3.4, and 4.0 orders of magnitude for *S. aureus*, *P. aeruginosa*, and *P. syringae*, respectively. As *S. aureus* is a Gram-positive bacterium, and *Pseudomonas* species are Gram-negative, this data suggest that RA_9R has a broad range of activity against both classes of bacteria.

For 0.05 wt % RA_6R, there is a small reduction in bacterial colony counts for *E. coli* and *P. aeruginosa* after 24 h. At 0.1 wt % RA_6R, there is a more significant effect against *P. aeruginosa*, denoted by a 4 log reduction in CFU after 24 h. However, there is no additional effect of 0.1 wt % RA_6R on *E. coli* or *S. aureus*. Interestingly, RA_6R is also strongly active against *P. syringae* with a log 4.5 reduction in CFU after 24 h, suggesting that RA_6R is more active against *Pseudomonas* bacteria.

For RA_6R acting against both *E. coli* and *P. aeruginosa* and RA_9R acting against *E. coli*, the main reduction in the number of CFUs occurs in the first 2 h after treatment with the peptide. However, in terms of RA_9R activity against *S. aureus*, this seems to occur steadily over the course of 24 h. The antimicrobial activity of these peptides is significantly lower than previously studied peptide RA_3R,[20] which in part may be due to the decreased concentrations used in this study, which were selected to correspond to concentrations where there is no substantial cytotoxicity. It can be seen that RA_9R displays little antimicrobial activity under these conditions. Interestingly, RA_6R displays a strong activity against *P. aeruginosa* at a concentration where the cytocompatibility (to fibroblasts) is acceptable.

CONCLUSIONS

We have systematically examined the self-assembly of two arginine-capped peptide bola-amphiphiles. Peptide RA_6R does not form self-assembled nanostructures, in contrast to RA_9R, which forms fibrils above a critical aggregation concentration, as imaged by cryo-TEM and as revealed by SAXS form factor fitting. Remarkably, these fibrils bind the "amyloid" specific dye ThT above a *cac* = 0.18 wt %, although circular dichroism and FTIR spectroscopy do not indicate β-sheet conformation below 1 wt % peptide. RA_9R does form β-sheet fibrils at high concentration as indicated by the data in Figure 2b and the CD spectrum for a dried sample as well as TEM images and SAXS data. This is also consistent with the observation that it forms a self-supporting hydrogel at sufficiently high concentration.

We then studied the interaction of the peptides with model DPPG/DPPE lipid membranes. DSC shows evidence for peptide-induced lipid demixing, especially in the DPPG rich mixtures, consistent with electrostatic interactions between this anionic lipid and the cationic arginine units in the peptides. CD spectra indicate no change of peptide conformation for RA_6R in the presence of lipids (PPII conformation retained), whereas unexpectedly RA_9R undergoes a transition to a β-sheet conformation in the presence of the lipids, possibly due to enhanced peptide concentration at the membrane interface. The DSC results suggest no significant influence of the peptides on T_m (DPPE), suggesting little penetration into the membrane, although ΔH does change, possibly indicating adsorption. This effect may be due to the low hydration of PE membranes resulting from strong lateral interactions of the lipids in the membrane, driven by hydrogen bonding of the head groups.[56,57] Stronger electrostatic interactions are expected for DPPG, as previously reported for other cationic antimicrobial peptides.[22,23,25,30,58]

Our initial antimicrobial screening study (and corresponding assay showing low cytotoxicity at the corresponding peptide concentration) shows that RA_6R is a promising antibacterial agent active against *P. aeruginosa*, strains of which (including those that have evolved antimicrobial resistance) can cause

DOI: 10.1021/acsabm.9b00172
ACS Appl. Bio Mater. XXXX, XXX, XXX−XXX

serious infections. The enhanced antibacterial activity of RA_6R compared to RA_9R may be due to the lower hydrophobicity of RA_6R, which, as we show by CD spectroscopy, also does not undergo a conformational switch in the presence of lipid membranes. Peptide RA_9R has a longer hydrophobic alanine sequence and self-assembles above a critical aggregation concentration and exhibits higher cytotoxicity under conditions where it is aggregated.

These arginine-rich peptide bola-amphiphiles show remarkable activity toward lipid membranes which is presumed to be the origin of their antimicrobial properties.

■ ASSOCIATED CONTENT

Supporting Information

The Supporting Information is available free of charge on the ACS Publications website at DOI: 10.1021/acsabm.9b00172.

SAXS fitting parameters, fluorescence assay spectra, additional CD data for RA_9R, RA_9R hydrogel SAXS and rheology data, temperature-dependent SAXS data for lipid/peptide mixtures, cryo-TEM images for lipid/peptide mixtures, low peptide concentration antimicrobial assay data (PDF)

■ AUTHOR INFORMATION

Corresponding Author

*E-mail: I.W.Hamley@reading.ac.uk.

ORCID

Valeria Castelletto: 0000-0002-3705-0162

Ian W. Hamley: 0000-0002-4549-0926

Notes

The authors declare no competing financial interest.

■ ACKNOWLEDGMENTS

We acknowledge Diamond Light Source and The University of Reading for funding CJCEG's studentship. I.W.H. thanks EPSRC for the award of a Platform grant (EP/L020599/1), which supported V.C. We thank the ESRF for the award of beamtime (ref SC4739) and Diamond Light Source for the award of beamtime (ref.sm18523-1). We thank Alessandro Mariani from ESRF, and Nathan Cowieson and Katsuaki Inoue (Diamond B21) for assistance during beamtime. We are grateful for access to the Chemical Analysis Facility at the University of Reading.

■ REFERENCES

(1) Dehsorkhi, A.; Castelletto, V.; Hamley, I. W. Self-Assembling Amphiphilic Peptides. *J. Pept. Sci.* **2014**, *20* (7), 453−467.

(2) Edwards-Gayle, C. J. C.; Hamley, I. W. Self-Assembly of Bioactive Peptides, Peptide Conjugates, and Peptide Mimetic Materials. *Org. Biomol. Chem.* **2017**, *15* (28), 5867−5876.

(3) Hamley, I. W. Self-Assembly of Amphiphilic Peptides. *Soft Matter* **2011**, *7* (9), 4122.

(4) Santoso, S.; Hwang, W.; Hartman, H.; Zhang, S. Self-Assembly of Surfactant-like Peptides with Variable Glycine Tails to Form Nanotubes and Nanovesicles. *Nano Lett.* **2002**, *2* (7), 687−691.

(5) Von Maltzahn, G.; Vauthey, S.; Santoso, S.; Zhang, S. Positively Charged Surfactant-like Peptides Self-Assemble into Nanostructures. *Langmuir* **2003**, *19* (10), 4332−4337.

(6) Hauser, C. A. E.; Zhang, S. Designer Self-Assembling Peptide Nanofiber Biological Materials. *Chem. Soc. Rev.* **2010**, *39* (8), 2780−2790.

(7) Vauthey, S.; et al. Molecular Self-Assembly of Surfactant-like Peptides to Form Nanotubes and Nanovesicles. *Proc. Natl. Acad. Sci. U. S. A.* **2002**, *99* (8), 5355−5360.

(8) Castelletto, V.; Edwards-Gayle, C. J. C.; Hamley, I. W.; Barrett, G.; Seitsonen, J.; Ruokolainen, J. Peptide-Stabilized Emulsions and Gels from an Arginine-Rich Surfactant-Like Peptide with Antimicrobial Activity. *ACS Appl. Mater. Interfaces* **2019**, *11* (10), 9893−9903.

(9) Castelletto, V.; Hamley, I. W.; Segarra-Maset, M. D.; Berdugo Gumbau, C.; Miravet, J. F.; Escuder, B.; Seitsonen, J.; Ruokolainen, J. Tuning Chelation by the Surfactant-like Peptide A_6H Using Predetermined pH Values. *Biomacromolecules* **2014**, *15* (2), 591−598.

(10) Castelletto, V.; Nutt, D. R.; Hamley, I. W.; Bucak, S.; Cenker, C.; Olsson, U. Structure of Single-Wall Peptide Nanotubes: In Situ Flow Aligning X-Ray Diffraction. *Chem. Commun.* **2010**, *46* (34), 6270−6272.

(11) Hamley, I. W.; Dehsorkhi, A.; Castelletto, V. Self-Assembled Arginine-Coated Peptide Nanosheets in Water. *Chem. Commun.* **2013**, *49* (18), 1850−1852.

(12) Castelletto, V.; Barnes, R. H.; Karatzas, K. A.; Edwards-Gayle, C. J. C.; Greco, F.; Hamley, I. W.; Rambo, R.; Seitsonen, J.; Ruokolainen, J. Arginine-Containing Surfactant-Like Peptides: Interaction with Lipid Membranes and Antimicrobial Activity. *Biomacromolecules* **2018**, *19* (7), 2782−2794.

(13) Castelletto, V.; Gouveia, R. M.; Connon, C. J.; Hamley, I. W.; Seitsonen, J.; Nykänen, A.; Ruokolainen, J. Alanine-Rich Amphiphilic Peptide Containing the RGD Cell Adhesion Motif: A Coating Material for Human Fibroblast Attachment and Culture. *Biomater. Sci.* **2014**, *2*, 362−369.

(14) Hamley, I. W.; Hutchinson, J.; Kirkham, S.; Castelletto, V.; Kaur, A.; Reza, M.; Ruokolainen, J. Nanosheet Formation by an Anionic Surfactant-like Peptide and Modulation of Self-Assembly through Ionic Complexation. *Langmuir* **2016**, *32* (40), 10387−10393.

(15) Chen, C.; Pan, F.; Zhang, S.; Hu, J.; Cao, M.; Wang, J.; Xu, H.; Zhao, X.; Lu, J. R. Antibacterial Activities of Short Designer Peptides: A Link between Propensity for Nanostructuring and Capacity for Membrane Destabilization. *Biomacromolecules* **2010**, *11* (2), 402−411.

(16) Dehsorkhi, A.; Castelletto, V.; Hamley, I. W.; Seitsonen, J.; Ruokolainen, J. Interaction between a Cationic Surfactant-like Peptide and Lipid Vesicles and Its Relationship to Antimicrobial Activity. *Langmuir* **2013**, *29* (46), 14246−14253.

(17) Zhao, Y.; Deng, L.; Yang, W.; Wang, D.; Pambou, E.; Lu, Z.; et al. Tuning One-Dimensional Nanostructures of Bola-Like Peptide Amphiphiles by Varying the Hydrophilic Amino Acids. *Chem. - Eur. J.* **2016**, *22* (32), 11394−11404.

(18) Zhao, Y.; Wang, J.; Deng, L.; Zhou, P.; Wang, S.; Wang, Y.; Xu, H.; Lu, J. R. Tuning the Self-Assembly of Short Peptides via Sequence Variations. *Langmuir* **2013**, *29* (44), 13457−13464.

(19) da Silva, E. R.; Walter, M. N. M.; Reza, M.; Castelletto, V.; Ruokolainen, J.; Connon, C. J.; Alves, W. A.; Hamley, I. W. Self-Assembled Arginine-Capped Peptide Bolaamphiphile Nanosheets for Cell Culture and Controlled Wettability Surfaces. *Biomacromolecules* **2015**, *16* (10), 3180−3190.

(20) Castelletto, V.; Barnes, R.; Karatzas, K.-A.; Edwards-Gayle, C. J. C.; Greco, F.; Hamley, I. W.; Seitsonen, J.; Ruokolainen, J. Restructuring of Lipid Membranes by an Arginine-Capped Peptide Bolaamphiphile. *Langmuir* **2019**, *35* (5), 1302−1311.

(21) Willumeit, R.; Kumpugdee, M.; Funari, S. S.; Lohner, K.; Navas, B. P.; Brandenburg, K.; Linser, S.; Andrä, J. Structural Rearrangement of Model Membranes by the Peptide Antibiotic NK-2. *Biochim. Biophys. Acta, Biomembr.* **2005**, *1669* (2), 125−134.

(22) Ishitsuka, Y.; Pham, D. S.; Waring, A. J.; Lehrer, R. I.; Lee, K. Y. C. Insertion Selectivity of Antimicrobial Peptide Protegrin-1 into Lipid Monolayers: Effect of Head Group Electrostatics and Tail Group Packing. *Biochim. Biophys. Acta, Biomembr.* **2006**, *1758* (9), 1450−1460.

(23) Arouri, A.; Dathe, M.; Blume, A. Peptide Induced Demixing in PG/PE Lipid Mixtures: A Mechanism for the Specificity of

DOI: 10.1021/acsabm.9b00172
ACS Appl. Bio Mater. XXXX, XXX, XXX−XXX

Antimicrobial Peptides towards Bacterial Membranes? *Biochim. Biophys. Acta, Biomembr.* **2009**, *1788* (3), 650−659.
(24) Malanovic, N.; Leber, R.; Schmuck, M.; Kriechbaum, M.; Cordfunke, R. A.; Drijfhout, J. W.; de Breij, A.; Nibbering, P. H.; Kolb, D.; Lohner, K. Phospholipid-Driven Differences Determine the Action of the Synthetic Antimicrobial Peptide OP-145 on Gram-Positive Bacterial and Mammalian Membrane Model Systems. *Biochim. Biophys. Acta, Biomembr.* **2015**, *1848* (10), 2437−2447.
(25) Neville, F.; Cahuzac, M.; Konovalov, O.; Ishitsuka, Y.; Lee, K. Y. C.; Kuzmenko, I.; Kale, G. M.; Gidalevitz, D. Lipid Headgroup Discrimination by Antimicrobial Peptide LL-37: Insight into Mechanism of Action. *Biophys. J.* **2006**, *90* (4), 1275−1287.
(26) Randle, C. L.; Albro, P. W.; Dittmer, J. C. The Phosphoglyceride Composition of Gram-Negative Bacteria and the Changes in Composition during Growth. *Biochim. Biophys. Acta, Lipids Lipid Metab.* **1969**, *187* (2), 214−220.
(27) Dowhan, W. Molecular Basis for Membrane Phospholipid Diversity: Why Are There so Many Lipids? *Annu. Rev. Biochem.* **1997**, *66*, 199−232.
(28) Brown, L.; Wolf, J. M.; Prados-Rosales, R.; Casadevall, A. Through the Wall: Extracellular Vesicles in Gram-Positive Bacteria, Mycobacteria and Fungi. *Nat. Rev. Microbiol.* **2015**, *13* (10), 620−230.
(29) Malanovic, N.; Lohner, K. Gram-Positive Bacterial Cell Envelopes: The Impact on the Activity of Antimicrobial Peptides. *Biochim. Biophys. Acta, Biomembr.* **2016**, *1858* (5), 936−946.
(30) Pimthon, J.; Willumeit, R.; Lendlein, A.; Hofmann, D. Membrane Association and Selectivity of the Antimicrobial Peptide NK-2: A Molecular Dynamics Simulation Study. *J. Pept. Sci.* **2009**, *15* (10), 654−667.
(31) Levine, H. Thioflavine T Interaction with Synthetic Alzheimer's Disease B-amyloid Peptides: Detection of Amyloid Aggregation in Solution. *Protein Sci.* **1993**, *2* (3), 404−410.
(32) LeVine, H. Quantification of β-Sheet Amyloid Fibril Structures with Thioflavin T. *Methods Enzymol.* **1999**, *309*, 274−284.
(33) Khurana, R.; Coleman, C.; Ionescu-Zanetti, C.; Carter, S. A.; Krishna, V.; Grover, R. K.; Roy, R.; Singh, S. Mechanism of Thioflavin T Binding to Amyloid Fibrils. *J. Struct. Biol.* **2005**, *151* (3), 229−238.
(34) Krebs, M. R. H.; Bromley, E. H. C.; Donald, A. M. The Binding of Thioflavin-T to Amyloid Fibrils: Localisation and Implications. *J. Struct. Biol.* **2005**, *149* (1), 30−37.
(35) Lindgren, M.; Sörgjerd, K.; Hammarström, P. Detection and Characterization of Aggregates, Prefibrillar Amyloidogenic Oligomers, and Protofibrils Using Fluorescence Spectroscopy. *Biophys. J.* **2005**, *88* (6), 4200−4212.
(36) Rambo, R. P. *Bioisis*, 2019. http://www.bioisis.net/.
(37) Breßler, I.; Kohlbrecher, J.; Thünemann, A. F. *SASfit*: A Tool for Small-Angle Scattering Data Analysis Using a Library of Analytical Expressions. *J. Appl. Crystallogr.* **2015**, *48* (5), 1587−1598.
(38) Blattner, F. R.; Plunkett, G.; Bloch, C. A.; Perna, N. T.; Burland, V.; Riley, M.; Collado-vides, J.; Glasner, J. D.; Rode, C. K.; Mayhew, G. F.; et al. The Complete Genome Sequence of Escherichia Coli K-12. *Science* **1997**, *277* (5331), 1453−1462.
(39) Horsburgh, M. J.; Aish, J. L.; White, I. J.; Shaw, L.; Lithgow, J. K.; Foster, S. J.; England, S. ΣB Modulates Virulence Determinant Expression and Stress Resistance: Characterization of a Functional RsbU Strain Derived from Staphylococcus Aureus 8325−4. *J. Bacteriol.* **2002**, *184* (19), 5457−5467.
(40) Holloway, B. Y. B. W. Genetic Recombination in Pseudomonas Aeruginosa. *Microbiology* **1955**, *13* (3), 572−581.
(41) Gasymov, O. K.; Glasgow, B. J. ANS Fluorescence: Potential to Augment the Identification of the External Binding Sites of Proteins. *Biochim. Biophys. Acta, Proteins Proteomics* **2007**, *1774* (3), 403−411.
(42) Chen, K.; Liu, Z.; Kallenbach, N. R. The Polyproline II Conformation in Short Alanine Peptides Is Noncooperative. *Proc. Natl. Acad. Sci. U. S. A.* **2004**, *101* (43), 15352−15357.
(43) Bochicchio, B.; Tamburro, A. M. Polyproline II Structure in Proteins: Identification by Chiroptical Spectroscopies, Stability, and Functions. *Chirality* **2002**, *14* (10), 782−792.
(44) Hirst, J. D.; Colella, K.; Gilbert, A. T. B. Electronic Circular Dichroism of Proteins from First-Principles Calculations. *J. Phys. Chem. B* **2003**, *107* (42), 11813−11819.
(45) Woody, R. W. Circular Dichroism Spectrum of Peptides in the Poly(Pro)II Conformation. *J. Am. Chem. Soc.* **2009**, *131* (23), 8234−8245.
(46) Schweitzer-Stenner, R.; Measey, T.; Hagarman, A.; Eker, F.; Griebenow, K. Salmon Calcitonin and Amyloid: Two Peptides with Amyloidogenic Capacity Adopt Different Conformational Manifolds in Their Unfolded States. *Biochemistry* **2006**, *45* (9), 2810−2819.
(47) Pelton, J. T.; Mclean, L. R. Spectroscopic Methods for Analysis of Protein Secondary Structure. *Anal. Biochem.* **2000**, *227* (2), 167−176.
(48) Gaussier, H.; Subirade, M.; Lavoie, M. C.; et al. Replacement of Trifluoroacetic Acid with HCl in the Hydrophobic Purification Steps of Pediocin PA-1: A Structural Effect. *Appl. Environ. Microbiol.* **2002**, *68* (10), 4803−4808.
(49) Ghosh, A.; Tucker, M. J.; Hochstrasser, R. M. Identification of Arginine Residues in Peptides by 2D-IR Echo Spectroscopy. *J. Phys. Chem. A* **2011**, *115*, 9731−9738.
(50) Barth, A. The Infrared Absorption of Amino Acid Side Chains. *Prog. Biophys. Mol. Biol.* **2000**, *74* (3−5), 141−173.
(51) Eker, F.; Cao, X.; Nafie, L.; Huang, Q.; Schweitzer-stenner, R. The Structure of Alanine Based Tripeptides in Water and Dimethyl Sulfoxide Probed by Vibrational Spectroscopy. *J. Phys. Chem. B* **2003**, *107* (1), 358−365.
(52) Schweitzer-Stenner, R. Dihedral Angles of Tripeptides in Solution Directly Determined by Polarized Raman and FTIR Spectroscopy. *Biophys. J.* **2002**, *83* (1), 523−532.
(53) Adochitei, A.; Drochioiu, G. Rapid Characterization of Peptide Secondary Structure by FT-IR Spectroscopy. *Rev. Roum. Chim.* **2011**, *56* (8), 783−791.
(54) Garidel, A. P.; Blume, A. Miscibility of Phosphatidylethanolamine-Phosphatidylglycerol Mixtures as a Function of pH and Acyl Chain Length. *Eur. Biophys. J.* **2000**, *28* (8), 629−638.
(55) Sevcsik, E.; Pabst, G.; Jilek, A.; Lohner, K. How Lipids Influence the Mode of Action of Membrane-Active Peptides. *Biochim. Biophys. Acta, Biomembr.* **2007**, *1768* (10), 2586−2595.
(56) Pink, D. A.; McNeil, S.; Quinn, B.; Zuckermann, M. J. A Model of Hydrogen Bond Formation in Phosphatidylethanolamine Bilayers. *Biochim. Biophys. Acta, Biomembr.* **1998**, *1368* (2), 289−305.
(57) Bouchet, A. M.; Frías, M. A.; Lairion, F.; Martini, F.; Almaleck, H.; Gordillo, G.; Disalvo, E. A. Structural and Dynamical Surface Properties of Phosphatidylethanolamine Containing Membranes. *Biochim. Biophys. Acta, Biomembr.* **2009**, *1788* (5), 918−925.
(58) Salay, L. C.; Ferreira, M.; Oliveira, O. N.; Nakaie, C. R.; Schreier, S. Headgroup Specificity for the Interaction of the Antimicrobial Peptide Tritrpticin with Phospholipid Langmuir Monolayers. *Colloids Surf., B* **2012**, *100*, 95−102.

DOI: 10.1021/acsabm.9b00172
ACS Appl. Bio Mater. XXXX, XXX, XXX−XXX